3D Printed X-band Evanescent Mode Waveguide Filter Based on Pixelization Strategy

Jaroslav Zechmeister and Jaroslav Lacik
Department of Radio Electronics, Faculty of Electrical Engineering and Communication, Brno University of Technology, 616 00 Brno, Czech Republic.
E-mail: Jaroslav.Zechmeister@vut.cz, lacik@vut.cz

A 3D-printed X-band evanescent mode waveguide filter based on pixelization strategy is proposed in this letter. The uniqueness of the filter lies in the exploitation of the evanescent mode waveguide in conjunction with a 3D-printed dielectric pixelated structure. The crucial advantage of this approach is the fact that the dielectric pixelated structure located in a waveguide is not metal coated, so the fabrication process is easier. The proposed filter is manufactured using the fused deposition modeling 3D print technology. Its measured transmission coefficient in the passband is approximately -2 dB, and the reflection coefficient is below -19 dB.

Introduction: Additive manufacturing, particularly 3D printing, stands at the forefront of a technological revolution, impacting various domains, including microwave technologies. The compelling advantages of 3D printing include not only speed but also the breadth of printing possibilities. This technology enables the fabrication of complex structures that were hitherto impracticable using traditional methods.

In recent years, a multitude of studies have unveiled the potential of 3D-printed waveguide filters [1-8]. For example, in [1], the selective laser melting (SLM) metal 3D printing technique is employed for crafting a waveguide filter based on cavity resonators. While SLM shows promise in Ku-band applications, at higher frequencies, a surface roughness might be a quite challenge. A stereolithography (SLA) 3D printing technology is able to print very precisely with good surface roughness. For instance, the publication [2] shows the leverage of SLA for producing a W-band waveguide bandpass filter, while [3] and [4] showcase Ka-band waveguide filters manufactured through SLA. Noteworthy is the application of SLA in crafting X-band waveguide filters. Notably, the work [5] introduces a monolithic 3D-printed filter with a twisted metal-insert bandpass design. 3D-printed filters based on spherical resonators and 3D-printed iris waveguide sections are presented in [6] and [7]. One limitation of these designs lies in the necessity for metal plating. In the realm of X-band waveguide filters, fused deposition modeling (FDM) 3D printing is also a possible choice. In [8] an extracted pole waveguide filter is presented and manufactured using the FDM. Customizable inserts to WR-90 waveguide, which may act as filters with desired frequency response, manufactured using the FDM are presented in [9]. In [10], a C-band filter integrating a single-ridge waveguide topology and EBG structure is presented. The examination of structural orientation's impact on filter parameters during the 3D printing process is meticulously detailed in [11]. Given that FDM primarily utilizes standard thermoplastic materials, the filters necessitate metal coating.

In our previous work [12], we proposed a procedure for designing a pixelated 3D-printed X-band waveguide filter. Since the filter was manufactured using the SLA 3D printing technology, metal coating of the individual parts of the filter, in our case by copper, was necessary. Unfortunately, a coating of the complex pixelated structure can be a challenging task. Thus, in this letter we propose an X-band waveguide filter, manufactured using the FDM 3D printing technology, that obviates the need for metal coating. Our inspiration stems from an evanescent mode filter presented in [13]. The evanescent mode waveguide realized as a WR-90 waveguide with a narrowed segment, accommodates a pixelated dielectric component. Realizing the desired frequency response involves the optimization of this pixelated component using the Binary Ink Stamp Optimization (BISO) algorithm. BISO is a heuristic algorithm tailored for optimizing pixelated structures [14]. It makes it possible to design the pixelated part of the filter without any predefined template and thus it can lead to unconventional solutions for the pixelated part shape. In stark contrast to the conventional filter design process, this approach is dependent solely on achieving the desired filter response. The absence of resonant mode computations or interconnection complexities streamlines the process. The filter's response is directly dependent on the dielectric pixelated component, optimized to attain the desired filter characteristics.

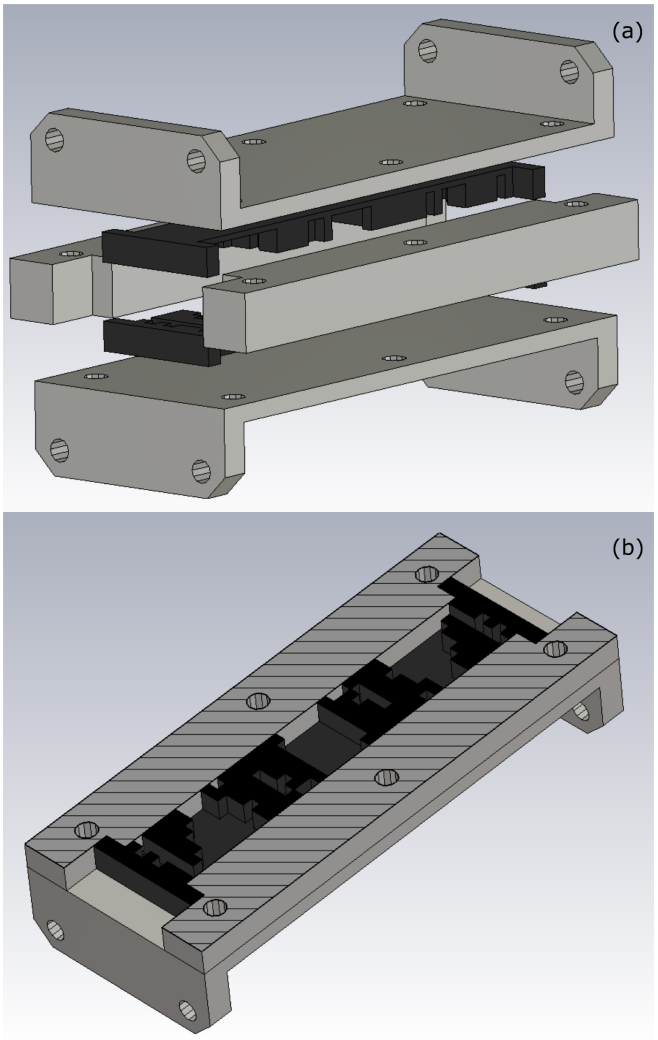

Fig 1 *Configuration of the proposed evanescent mode waveguide filter with pixelated structure (a) and its cross-section (b).*

Design and Optimization: The configuration of the proposed filter, as depicted in Fig 1, is founded on a 100 mm long piece of WR-90 waveguide with dimensions of a width a=22.86 mm and a height b=10.16 mm. This waveguide features an integrated narrowed section, measuring 14 mm in width, fashioned to elevate the cut-off frequency of the fundamental TE10 mode. Consequently, the operational frequency band of the filter lies below this cut-off frequency. To realize the desired response characteristics of the filter, a 3D-printed pixelated component is inserted into this narrowed section. This pixelated component encompasses a grid of 7×40 positions, each with the potential to be filled with material or left void. Each individual pixel takes the form of a block with a 2×2 mm^2 square base and a height of 10.16 mm.

For designing the pattern of the pixelated component, we employed the Binary Ink Stamp Optimization (BISO) algorithm. BISO is a heuristic algorithm designed for optimizing pixelated structures [14]. The concept behind the algorithm is inspired by ink stamps with varying ink saturation levels. In each iteration (limited by a maximum number of iterations denoted as $Niter$), each individual (totaling a number of individuals in each iteration designated by $Npop$) undergoes evaluation using a fitness function. A set of elite individuals with the best fitness values is then selected (the number of elite individuals is denoted as $Nelit$). This elite group can be likened to a collection of ink stamps, where saturation levels correlate with their fitness values. The subsequent generation

$$F_{S11} = \frac{1}{N}\sum_{n=1}^{N}\begin{cases} \frac{0.941-S11_n}{0.944} & \text{if} \quad S11_n < 0.944 \quad \& \ (f_n \le 9 \text{ OR } f_n \ge 9) \\ \frac{0.708-S11_n}{0.708} & \text{if} \quad S11_n < 0.708 \quad \& \ (9 < f_n \le 9.5 \text{ OR } 10.5 \le f_n < 9) \\ \frac{S11_n-0.177}{0.823} & \text{if} \quad S11_n > 0.177 \quad \& \ (9.6 < f_n < 10.4) \\ 0 & \text{else} \end{cases} \tag{2}$$

$$F_{S21} = \frac{1}{N}\sum_{n=1}^{N}\begin{cases} \frac{S21_n-0.1}{0.9} & \text{if} \quad S21_n > 0.1 \quad \& \ (f_n \le 9 \text{ OR } f_n \ge 9) \\ \frac{S21_n-0.708}{0.292} & \text{if} \quad S21_n > 0.708 \quad \& \ (9 < f_n \le 9.5 \text{ OR } 10.5 \le f_n < 9) \\ \frac{0.944-S21_n}{0.944} & \text{if} \quad S21_n < 0.944 \quad \& \ (9.6 < f_n < 10.4) \\ 0 & \text{else} \end{cases} \tag{3}$$

Table 1. Parameters setting for BISO algorithm during fillter optimization.

Parameter	Value
$Nelit$	5
$Niter$	250
$Npop$	50
$minProb$	0.005
$minProbRST$	0.15
$sigCoeff$	10

is determined through a probability matrix, which can be imagined as an imprint of all stamps over each other. The matrix's darker areas correspond to higher probabilities of generating "1," while brighter regions indicate a greater likelihood of generating "0." The parameter $minProb$ establishes the minimum probability for generating "1." If the algorithm becomes trapped in a local minimum, $minProb$ is adjusted to $minProbRST$. The $sigCoeff$ parameter governs the steepness of a sigmoid function used to transform the fitness function into ink saturation levels.

The BISO algorithm enables the design of the pixelated part of the filter without relying on predefined templates or a resonant initial structure. Given the symmetry of the pixelated section, the optimized binary matrix comprised 7×20 bits. The filter was designed to have a 1 GHz bandwidth at the center frequency of the X-band (10 GHz), a passband transmission coefficient more than -0.5 dB, and a reflection coefficient of -15 dB. The cost function was devised in relation to the restricted zones (masks) within the S11 and S21 filter response. For each individual, the cost value was calculated as a sum of penalties for each frequency point. If the S11 or S21 filter response intersected with these restricted areas, the value exceeded zero. Alternatively, the fitness function could be determined using a zeros and poles approach, where the desired filter response is represented by zeros and poles. The fitness function was defined as:

$$F = \sqrt{{F_{S11}}^2 + {F_{S21}}^2}, \tag{1}$$

where F_{S11} and F_{S21} are sub-fitness functions defined in equations (2) and (3). In Equations (2) and (3), N represents the number of frequency points, f_n signifies the frequency at a given point in GHz, while $S11_n$ and $S21_n$ correspond to the magnitudes in a linear scale of the reflection and transmission coefficients at that frequency point. The parameters of the BISO algorithm were configured as illustrated in Table 1. After conducting multiple trial runs of the optimization process, these parameters were selected to achieve an optimal balance between the algorithm's exploratory and exploitative capabilities for this specific task.

The S11 and S21 parameters were derived from comprehensive full-wave electromagnetic simulations performed using CST Studio Suite. These parameters were then utilized to compute the fitness function through an in-house Matlab script. The optimization process itself was also managed by a custom in-house Matlab code. The resultant optimized pixelated structure is depicted in Fig 2.

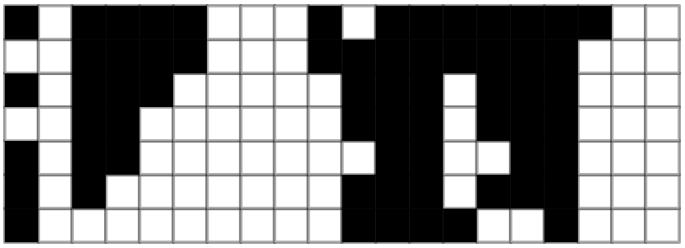

Fig 2 *Optimized binary matrix.*

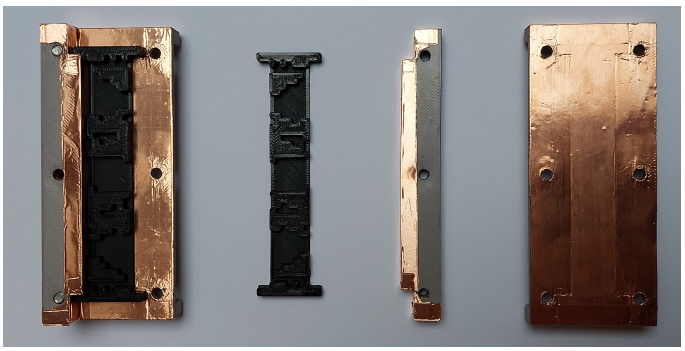

Fig 3 *Manufactured prototype of the filter.*

Fabrication and Measurement: For the sake of simplifying the manufacturing process, the optimized pixelated component was produced in two sections (Fig 1 a)). Fabrication was carried out using a low-cost FDM 3D printer, specifically the Prusa MK3 model, while the chosen filament material was XT copolyester from Colorfabb [15]. This material was selected due to its relatively low dielectric losses when compared to other commonly used thermoplastic filaments [16]. Notably, its dielectric constant is 2.85 and the loss tangent is 0.0053. Since we want to decrease the production time of the prototype, the evanescent mode waveguide was also 3D printed and subsequently coated with a layer of copper foil (Fig 3). Given its relatively simple geometry, this part can be alternatively manufactured using a CNC milling machine. Moreover, a waveguide piece with an appropriate cut-off frequency could also serve as a suitable substitute for this component.

The manufactured prototype of the proposed filter was measured using a vector network analyzer Rohde & Schwarz ZVA67. The comparison between measured and simulated results is presented in Fig 4. The measured transmission coefficient within the passband is approximately -2 dB, and the reflection coefficient remains below -19 dB. The mea-

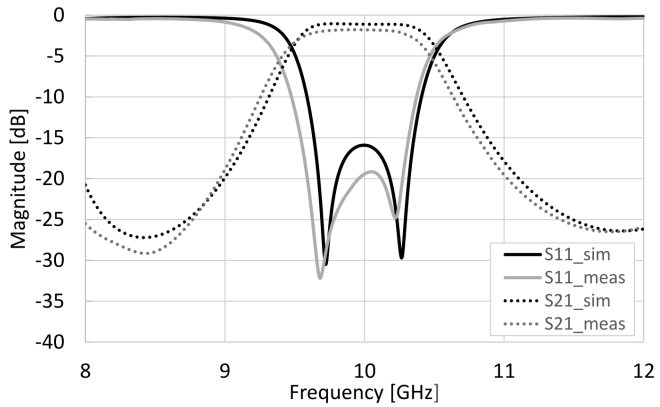

Fig 4 *Simulated and measured results of the proposed filter.*

Table 2. Simulated transmission coefficient based on loss tangent.

Loss tangent [-]	Transmission coefficient [dB]
0	-0.14
0.0025	-0.6
0.005	-1.06
0.0075	-1.53
0.01	-1.99

sured pass bandwidth spans 1.041 GHz (from 9.42 GHz to 10.46 GHz). A minor discrepancy between the simulated and measured responses can be attributed to inherent limitations in the manufacturing process.

Unlike conventional state-of-the-art 3D-printed X-band waveguide filters, our innovative design obviates the necessity for a metal coating on the intricate 3D-printed structure. The metallization process for such complex dielectric structures may be quite a challenge. Achieving a uniform metalized layer on intricately shaped surfaces is particularly demanding. Furthermore, a metal 3D-printed filter may require additional plating due to its inherently low surface conductivity. In addition, surface roughness could potentially be a significant issue, especially at higher frequencies. Moreover, the performance of our filter relies solely on the geometry of the 3D-printed dielectric insert. This unique characteristic grants the flexibility to fine-tune its response simply by substituting the insert, offering unparalleled versatility.

Thanks to the utilization of low-cost thermoplastic material in the fabrication process, the passband transmission coefficient is somewhat affected by the relatively higher loss tangent of the material. However, this limitation can be effectively addressed by leveraging specialized 3D printing filaments designed for RF applications. Encapsulated in the table, we have summarized simulated passband transmission coefficients based on varying loss tangents. Notably, employing XT copolyester with a loss tangent of 0.0053 should theoretically yield a transmission coefficient of approximately -1.1 dB. It's worth mentioning that the additional loss observed might have been due to the imperfect realization of the waveguide structure. Alternatively, employing CNC manufacturing for the waveguide, coupled with materials possessing a suitable loss tangent, should make it feasible to achieve a passband transmission coefficient of -0.5 dB.

Conclusion: An evanescent mode 3D-printed X-band waveguide filter, employing a pixelization strategy, has been meticulously developed and presented. The distinguishing feature of this filter resides in its adept utilization of the evanescent mode waveguide, synergistically integrated with a 3D-printed dielectric pixelated structure. This innovative approach obviates the necessity for metal coating on the 3D-printed component. Through a judicious optimization of the pixelated structure's geometry, we achieved the targeted frequency response for the filter. It's worth emphasizing that this design methodology exhibits remarkable versatility, and any potential constraints should be a subject for exploration in forthcoming research endeavors.

Acknowledgments: This work was supported by the Internal Grant Agency of The Brno University of Technology, project no. FEKT-S-23-8191.

Received: DD MMMM YYYY *Accepted:* DD MMMM YYYY
doi: 10.1049/ell.10001

References

1. Vaitukaitis, P., et al.: On the development of metal 3d printed bandpass filter with wide stopband based on deformed elliptical cavity resonator with an additional plate. IEEE access 10, 15427–15435 (2022)
2. Shang, X., et al.: *w* -band waveguide filters fabricated by laser micromachining and 3-d printing. IEEE Transactions on Microwave Theory and Techniques 64(8), 2572–2580 (2016). doi:10.1109/TMTT.2016.2574839
3. Zhang, Y., et al.: A 3-d printed ka-band twisted waveguide filter with filtering and polarization rotation. In: 2019 IEEE International Symposium on Antennas and Propagation and USNC-URSI Radio Science Meeting, pp. 1701–1702. IEEE (2019)
4. Zhang, Y., et al.: 3d printed waveguide step-twist with bandpass filtering functionality. Electronics letters 56(11), 527–528 (2020)
5. Bartlett, C., et al.: X-band 3d-printed metal-insert twist-component for bandpass filter applications. In: 2021 IEEE MTT-S International Microwave Filter Workshop (IMFW), pp. 329–331. (2021)
6. Guo, C., et al.: A 3-d printed lightweight x-band waveguide filter based on spherical resonators. IEEE microwave and wireless components letters 25(7), 442–444 (2015)
7. Ghazali, M.I.M., et al.: 3d printed metalized plastic waveguides for microwave components. International Symposium on Microelectronics 2017(1), 000078–000082 (2017)
8. Miek, D., et al.: Additive manufacturing of e-plane cut extracted pole waveguide filters with frequency-dependent coupling apertures. In: 2020 IEEE Asia-Pacific Microwave Conference (APMC), pp. 522–524. (2020)
9. Dahle, R., Laforge, P., Kuhling, J.: 3-d printed customizable inserts for waveguide filter design at x-band. IEEE microwave and wireless components letters 27(12), 1080–1082 (2017)
10. García-Martínez, H., et al.: 3d-printed electromagnetic band-gap bandpass filter based on empty single-ridge waveguide. IEEE Access 10, 53954–53962 (2022). doi:10.1109/ACCESS.2022.3175868
11. Bruhn, D., et al.: Effects of cutting planes on filter performance of fdm 3d-printed x-band waveguide filters. In: 2021 IEEE MTT-S International Microwave Filter Workshop (IMFW), pp. 236–238. (2021)
12. Zechmeister, J., Lacik, J.: Automatic design procedure of waveguide filters based on a pixelization strategy. IEEE Microwave and Wireless Technology Letters 33(10), 1423–1425 (2023). doi:10.1109/LMWT.2023.3297514
13. Pons, A., et al.: Evanescent mode filters composed of dielectric parts built using 3d-printing methods. In: 2021 IEEE MTT-S International Microwave Filter Workshop (IMFW), pp. 14–16. (2021)
14. Zechmeister, J., Lacik, J., Kadlec, P.: The design of pixelated siw horn antennas with nearly equal beamwidths using binary ink stamp optimization. IEEE access 9, 122216–122227 (2021)
15. Colorfabb. https://colorfabb.com/filaments/materials
16. Zechmeister, J., Lacik, J.: Complex relative permittivity measurement of selected 3d-printed materials up to 10 ghz. In: 2019 Conference on Microwave Techniques (COMITE), pp. 1–4. (2019)